ACS Catalysis

Research Article

Cite This: ACS Catal. 2019, 9, 5365−5374

pubs.acs.org/acscatalysis

Ultralow Loading and High-Performing Pt Catalyst for a Polymer Electrolyte Membrane Fuel Cell Anode Achieved by Atomic Layer Deposition

Zhongxin Song,[†,‡] Mohammad Norouzi Banis,[†] Hanshuo Liu,[∥] Lei Zhang,[†] Yang Zhao,[†] Junjie Li,[†] Kieran Doyle-Davis,[†] Ruying Li,[†] Shanna Knights,[§] Siyu Ye,[§] Gianluigi A. Botton,[*,∥] Ping He,[*,§] and Xueliang Sun[*,†]

[†]Department of Mechanical and Materials Engineering, University of Western Ontario, London, ON N6A 5B9, Canada

[‡]College of Materials Science and Engineering, Shenzhen University, Shenzhen 518060, China

[§]Ballard Power Systems Inc., 9000 Glenlyon Parkway, Burnaby, BC V5J 5J8, Canada

[∥]Department of Materials Science and Engineering, McMaster University, Hamilton, Ontario L8S 4L8, Canada

Supporting Information

ABSTRACT: Decreasing Pt loading in the anode layer below ~0.025 mg·cm^{-2} is found to reduce the hydrogen oxidation reaction rate during polymer electrolyte membrane fuel cells (PEMFCs) normal operation, when using conventional Pt/C catalysts and electrode coating methods. To achieve extremely low Pt loading in the anode catalyst layer while maintaining high PEMFC performance and durability, a series of membrane electrode assemblies (MEAs) with low Pt loading in the anode layer are successfully prepared using an atomic layer deposition (ALD) technique. When the ALD cycle number is controlled, the Pt nanoparticles (NPs) with different sizes and loadings are directly deposited on the carbon layer to form the anode catalyst layer. The ALDPt NPs with uniform particle sizes are highly distributed on the carbon surface, which promotes the ALDPt with high electrochemical active surface area and enables enhanced performance of ALDPt-MEAs. Particularly, the 50ALDPt-MEA with the anode Pt prepared by 50ALD cycles shows excellent H_2−air PEMFC activity and durability. Importantly, the 20ALDPt-MEA with an ultralow anode Pt loading of 0.01 mg·cm^{-2} displays a significantly high surface area of 155 $m^2 \cdot g^{-1}_{Pt}$, approximately 3 times higher than the 50.3 $m^2 \cdot g^{-1}_{Pt}$ for commercial Pt catalyst. The 20ALDPt anode also shows better stability than that of the commercial Pt/C during the anode potential cycling test. The ultralow Pt loading, uniform Pt distribution, high MEA performance, and durability achieved indicate that the ALD technique has great potential in developing high-performing electrocatalysts for PEMFC.

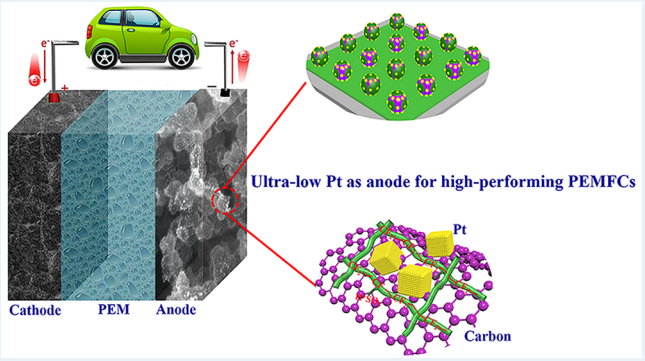

KEYWORDS: *ultralow Pt loading, polymer electrolyte membrane fuel cell, membrane-electrode assembly, startup and shutdown cycling, atomic layer deposition*

Downloaded via WESTERN UNIV on September 12, 2019 at 18:51:32 (UTC).
See https://pubs.acs.org/sharingguidelines for options on how to legitimately share published articles.

1. INTRODUCTION

Polymer electrolyte membrane fuel cells (PEMFCs) are some of the most efficient devices for converting the stored chemical energy from hydrogen into useable electrical energy, making it a key technology as society transitions toward clean energy.[1] Unfortunately, the current electrode catalyst layers in PEMFCs require high loading of platinum-based (Pt) noble metal catalysts to drive the desired electrochemical reactions (hydrogen oxidation reaction (HOR) at the anode, and oxygen reduction reaction (ORR) at the cathode).[2] Therefore, it is of great interest and importance to reduce the loading of noble metal catalysts to make PEMFCs cost-competitive in the field of clean energy.[3] The U.S. Department of Energy (DOE) is targeting a total Pt loading of 0.125 mg·cm^{-2} by 2020 to meet cost requirements,[4] allowing only 0.025 mg·cm^{-2} for the anode, which is the lowest loading achievable by conventional electrode preparation methods without reducing HOR kinetics.[1d,5] The fast HOR kinetics on supported Pt catalyst (Pt/C) requires a very small amount of anode catalyst.[6] However, when lowering the Pt loading to less than 0.025 mg·cm^{-2}, a conventionally coated anode could result in reduced HOR performance in MEA due to the very thin layer thickness. If a low Pt content (<50% Pt/C) catalyst is used to increase the layer thickness and reduce the active site

Received: November 8, 2018
Revised: March 15, 2019
Published: April 15, 2019

© 2019 American Chemical Society

DOI: 10.1021/acscatal.8b04504
ACS Catal. 2019, 9, 5365−5374

density, the proton and the electric conductivities could be problematic. Furthermore, the cycling durability of the low Pt loading anodes in air/air startup/shutdown (SUSD) could become another critical failure mode.[5e,7] For example, during the PEMFC air/air SUSD process, the anode potential may vary from ∼0 to ∼1.0 V or even higher (vs RHE) when the anode channel gas alternates from hydrogen rich fuel to air. This potential variation will lead to active surface area loss of the Pt nanoparticles (NPs) catalyst.[8] It is reported that the anode potential increased rapidly when the anode is starved of H_2, and soon became higher than the cathode potential, which leads to cell reversal.[9] In this high anode potential condition, water electrolysis and even carbon corrosion reactions can take place. The carbon corrosion at the anode could weaken the attachment of Pt particles to the carbon support, decrease the electronic continuity of the catalyst layer, and eventually lead to severe Pt agglomeration and cell performance degradation. The phenomenon would be more severe in anodes with ultralow Pt loading and negatively affect the PEMFCs performance and durability. Although great progress has been achieved in lowering Pt loading from 0.4 mg/cm^2 to state-of-the-art 0.05 mg/cm^2 in the anode layer, few efforts concern the anode stability during SUSD operation and fuel starvation scenario when low Pt loading (<0.05 mg/cm^2) anodes are used.[10] Therefore, pursuing a new technology to prepare the electrode catalyst layer with not only low Pt loading but also excellent performance and durability is necessary to develop the low-cost PEMFCs.

Direct deposition of Pt NPs on the surface of carbon-coated layer is an efficient way in preparing the highly effective electrocatalysts for fuel cells, because it can promote the exposure of Pt active surface and enhance the Pt utilization in the membrane electrode assembly (MEA).[10a,b,d,11] Among the reported methods for Pt catalyst preparation, atomic layer deposition (ALD) emerged as an attractive technique due to the advantages, high dispersion, and precise size control.[12] Theoretically, the self-limiting reaction nature[12d,13] of ALD enables the achievement of monolayer dispersion of metal atoms on the substrate, which makes ALD an attractive technique for preparing Pt NPs in PEMFCs electrode with high dispersion and controllable loading. To date, few studies have reported the ALD of highly dispersed Pt or transition metal oxide NPs for PEMFCs application. Sun et al. prepared Pt NPs on different carbon supports by the ALD method, and the synthesized ALDPt-CNTs or ALDPt-Graphene are used as electrocatalysts for ORR, methanol oxidation, and water splitting, which show significantly enhanced electrocatalytic activity.[12c,14] However, direct deposition of the Pt NPs on the electrode carbon with three-phase boundary (Pt-carbon-ionomer) by ALD has not been studied yet. Additionally, there is a lack of investigations of the low ALDPt loading impact on the PEMFCs performance and durability.

In this work, ALD technology is used for the first time to deposit ultralow Pt loading on the bonded carbon layer, by which the Pt NPs are directly deposited onto the surface of carbon to form the anode catalyst layer with three-phase boundary (Pt-carbon-ionomer). The novelty of post deposition of Pt on the PEMFC anode layer is that it can effectively improve the Pt utilization and enhance the PEMFC performance while reducing the Pt loading. Through controlling the number of ALD cycles (50, 30 and 20), a series of anode layers with different Pt loadings and particle sizes are obtained. The MEA assembled with ALDPt catalyst in the anode showed much better H_2−air PEMFC performance and durability than the MEA prepared with the commercial catalyst (46 wt % Pt/C) through a conventional method. The uniform Pt distribution and excellent H_2−air PEMFCs performance and durability indicate that a PEMFC with ultralow Pt loading achieved by ALD holds promise a scalable platform in developing of high-performance and low-cost PEMFCs.

2. EXPERIMENTAL PROCEDURES

2.1. ALD of Pt NPs on a Bonded Carbon Layer. A bonded carbon layer provided by Ballard Power Systems, Inc. was used as the substrate for Pt deposition. The bonded carbon layer is prepared by coating 20 wt % Nafion/carbon black ink on the PTFE sheets with the carbon layer thickness of 1.0 um after drying. Pt NPs were deposited on the bonded carbon layers by the ALD method (Cambridge Nanotechnology Inc.) using (methylcyclopentadienyl)Pt^{IV}trimethyl ($MeCpPtMe_3$) and O_2 as precursors in a procedure similar to that in our previously reported work.[12b,c,15] $MeCpPtMe_3$ and O_2 were alternatively introduced into the ALD chamber for Pt deposition. The bubbler of $MeCpPtMe_3$ precursor was heated to 65 °C while O_2 was kept at room temperature, in order to provide enough vapor for ALDPt. Delivery lines were heated to 150 °C to prevent the precursors from condensation. Nitrogen gas (99.999% in purity) was used as a carrier gas at a flow rate of 20 sccm, and the ALD chamber was maintained at a low level of base pressure (typically 0.3−0.4 Torr) by a vacuum pump. The bonded carbon layer with the sheet size of 10 cm × 10 cm was placed in the ALD chamber, and the deposition temperature was 250 °C. One ALD cycle was executed with the completion of following six steps: (1) a 0.5 s supply of $MeCpPtMe_3$; (2) a 5.0 s extended exposure of $MeCpPtMe_3$ in the ALD chamber; (3) a 20 s purge of excess $MeCpPtMe_3$ and any byproducts; (4) 1.0 s supply of O_2; (5) a 5.0 s extended exposure of O_2 in the ALD chamber; (6) a 20 s purge of excess O_2 and any byproducts. The ALD Pt was prepared by repeating the above ALD of 50, 30, and 20 cycles, and the Pt loading was measured by the technique of inductively coupled plasma-optical emission spectroscopy (ICP-OES). First, the slices with the diameter of 1.0 cm were cut off from the ALDPt-carbon layer in different locations; the area of each slice is 0.785 cm^2. Then four slices of the ALDPt-carbon layer with the total area of 3.14 cm^2 were put into 10 mL aqua regia ($HCl:HNO_3$ = 3:1) to completely dissolve the Pt nanoparticle overnight. Finally, the 1.0 mL aqua regia with dissolved Pt was diluted with 9.0 mL of H_2O, and then it was used to measure the Pt concentration by the ICP-OES. From the ICP-OES, the Pt loadings of 0.035, 0.02, 0.01 mg·cm^{-2} were achieved with 50, 30, and 20 ALD cycles, respectively. The Pt loading in the commercial 46 wt % Pt/C coated anode was detected by the ICP-OES with the same condition and 0.035 mg·cm^{-2} Pt loading was revealed. On the basis of the Pt loading and carbon loadings (0.04 mg·cm^{-2}) on the anode layer, the weight percent of Pt on carbon can be calculated to be ∼46 wt %, ∼33 wt %, and ∼20 wt % for 50ALD, 30ALD, and 20ALD preparation, respectively.

2.2. MEA Preparation and Single Fuel Cell Performance Testing. Prior to fabricating the MEA, a catalyst-coated membrane (CCM) was prepared by a decal transfer method. The cathode was fabricated using a Ballard standard research Pt/C catalyst with a thickness of 10 μm and Pt loading of 0.4 mg·cm^{-2}. The membrane used in this report was Chemours (formerly DuPont) Nafion PFSA NR-211 (thickness of ∼25

DOI: 10.1021/acscatal.8b04504
ACS Catal. 2019, 9, 5365−5374

um). The anode catalyst layer with a thickness of ~1 μm and Pt NPs deposited by ALD was decal transferred onto the Nafion membrane by hot-pressing, after a layer of Nafion was sprayed onto the catalyst. Finally, the CCM was sandwiched between two gas diffusion layers (GDLs) and assembled with a gasket frame for an active area of 45 cm^2. To understand the Pt loading impact on anodic HOR activity and investigate the lower limiting of anode Pt loading for the PEMFC application, the MEAs composed with ALDPt anodes with loadings of 0.035, 0.02, 0.01 $mg{\cdot}cm^{-2}$ and cathodes with 0.4 $mg{\cdot}cm^{-2}$ Pt/C were prepared. Additionally, the MEA made by commercial 46 wt % Pt/C with Pt loading of 0.4 $mg{\cdot}cm^{-2}$ for cathode and 0.035 $mg{\cdot}cm^{-2}$ for anode was fabricated for comparison.

The MEA single cell performance testing was conducted under conditions of 75 °C, 5 psig, 100% relative humidity (RH), with anode feed of hydrogen and cathode of air at flow rates of 2 and 4 slpm, respectively. Before testing, MEA conditioning was performed at a current density of 1.3 $A{\cdot}cm^{-2}$ for 16 h. The PEMFC H_2−air polarization curves were recorded on a Ballard standard research fuel cell test stations. Each testing polarization point was allowed to stabilize at the setting current for 5 min, and the reported voltage data was the average of the last 30 s. Moreover, to understand the active surface area of the anode catalyst, the cyclic voltammetry (CV) with CO stripping was carried out on the MEA anode side. The polarization curves of the MEA anode catalyst for hydrogen oxidation were determined. To evaluate the durability and lifetime of the anode catalyst, an anode potential cycling protocol using a square wave potential control with 30 s intervals each of holding at 0.1 and 1.0 V (vs RHE) was performed to mimic the possible anode performance degradation in start-up/shutdown processes. During the accelerated stress test (AST), the anode fed with N_2 served as the working electrode, while the cathode under the H_2 atmosphere worked as the counter electrode. In this cycling protocol, the cathode was constantly soaked in the 100% H_2 and was not expected to have significant catalyst degradation. The working electrode of the anode, however, went through an electrochemical potential alternating between 0.1 and 1.0 V. A total of 2000 AST cycles were performed on the anodes and intermediate performance monitoring was conducted via air polarization curves, power density, and anode electrochemical catalyst active surface area (ECSA) loss.

2.3. Materials Characterization. The morphology and microstructure of Pt NPs were characterized by high-resolution transmission electronic microscopy (HRTEM, JEOL 2010FEG) and a Hitachi S-4800 field emission scanning electronic microscope (FESEM). The Pt loading on anode layers prepared by ALD was determined by ICP-OES. The TEM cross-section samples of MEAs were prepared using an ultramicrotome (Leica Ultracut UCT) with a DiATOME diamond knife at a thickness of ~70 nm. The structural and elemental analysis of the cross-section samples were carried out using a FEI Titan Cubed 80−300 kV microscope equipped with spherical aberration correctors (probe and imaging forming lenses) operated at 200 kV. The scanning transmission electronic microscopy (STEM) images equipped with the energy-dispersive X-ray spectroscopy (EDX) were acquired by a high-angle annular dark field (HAADF) detector with a collection angle ~64−200 mrad.

3. RESULTS AND DISCUSSION

3.1. Structural Characterization. Scheme 1 presents the deposition of Pt NPs on the bonded carbon layers using the ALD technique. By controlling the number of ALD cycles, different designs of Pt loading can be achieved on the carbon layers, forming the anode catalyst layers for PEMFC application. After ALD of Pt NPs, the anode catalyst layer was sprayed with a layer of Nafion ionomer and decal transferred to the Nafion membrane by a hot-pressing method to obtain the CCM. Subsequently, by assembling the CCM with GDLs, the MEA single cell can be fabricated. From the TEM images (Figure 1) and SEM images (Figure S1), it is found that the Pt particle size and loading amount can be precisely controlled by varying the ALD cycles. For the commercial Pt/C catalyst with the 0.035 $mg{\cdot}cm^{-2}$ Pt loading, the Pt NPs with an average size of 3.5 nm tend to aggregate along the edges and defect sites presumably at low energy sites (Figure 1a and Figure S1a). In contrast, highly uniform dispersion of Pt NPs with the same loading of 0.035 $mg{\cdot}cm^{-2}$ can be achieved on the carbon layers by 50ALD cycles, with the average Pt NPs size of 3.2 nm (Figure 1b and Figure S1b). Therefore, we observe that the ALD provides significant advantages in uniform deposition of Pt NPs on the available carbon surface. By decreasing the number of ALD cycles to 30, a lower Pt loading of 0.02 $mg{\cdot}cm^{-2}$ and smaller Pt particle size of 2.3 nm can be deposited on the carbon layers (Figure 1c and Figure S1c). To further enable the ultralow Pt loading to 0.01 $mg{\cdot}cm^{-2}$, 20 ALD cycles are applied to construct the Pt NPs on carbon layers. The HRTEM image in Figure 1d and SEM image in Figure S 1d indicate that Pt NPs with the average size of 1.5 nm are deposited on the carbon support with a homogeneous distribution on the carbon surface.

Scheme 1. Schematic Illustration for Atomic Layer Deposition (ALD) of Pt NPs on Bonded Carbon Layers

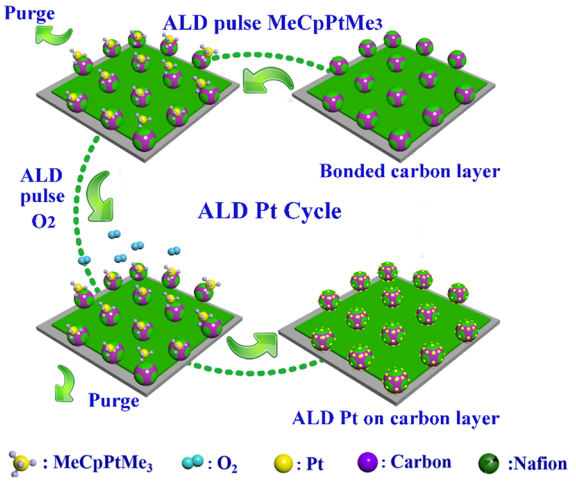

3.2. PEMFCs Performance with ALDPt Catalysts. To understand the anode Pt loading impact on single cell performance, a series of MEAs with anode/cathode Pt loadings of 0.035/0.4, 0.02/0.4, and 0.01/0.4 $mg{\cdot}cm^{-2}$, in which the anode Pt catalyst is made by ALD and a cathode of commercial 46 wt % Pt/C are prepared. In Figure 2a, the beginning-of-life (BOL) performance of H_2−air polarization curves for MEAs with different anode Pt loadings are displayed. It is noticed that all the MEAs show the open circuit voltage (OCV) with a high

DOI: 10.1021/acscatal.8b04504
ACS Catal. 2019, 9, 5365−5374

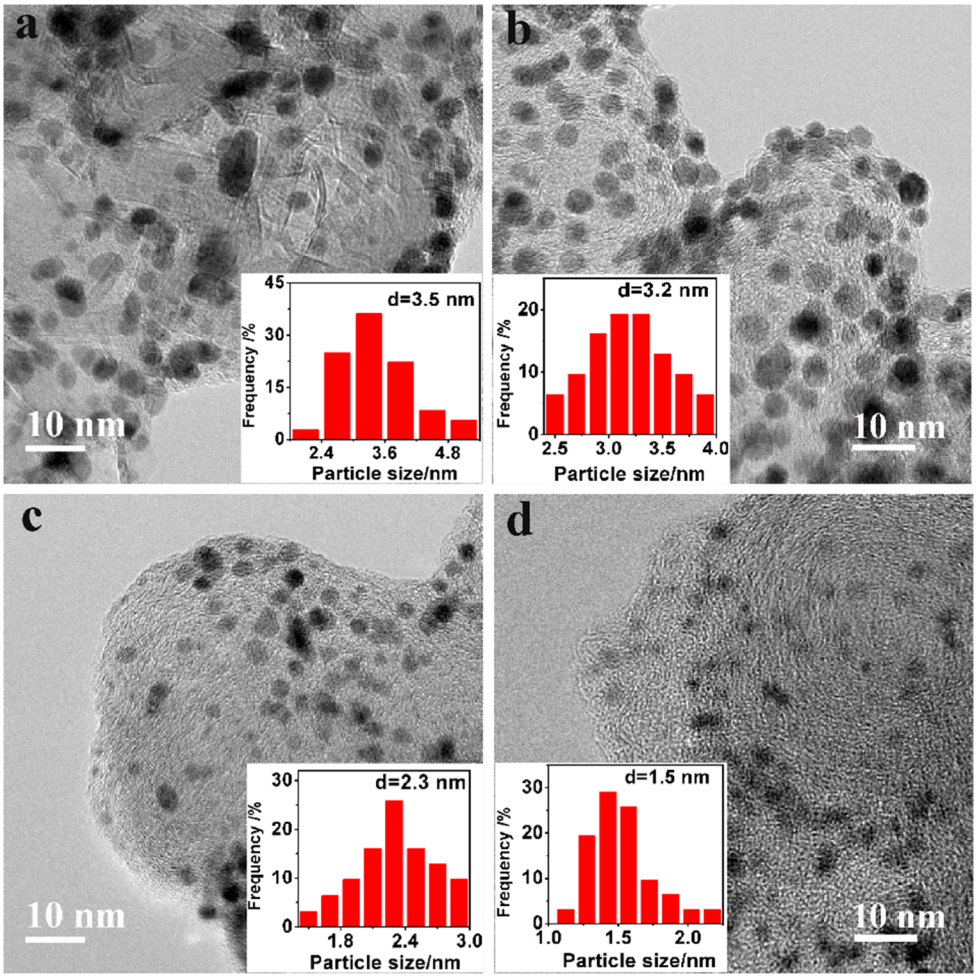

Figure 1. HRTEM images and corresponding size distribution histogram of anode catalyst layer with Pt NPs made by (a) commercial Pt/C, (b) 50ALD Pt, (c) 30ALD Pt, and (d) 20ALD Pt.

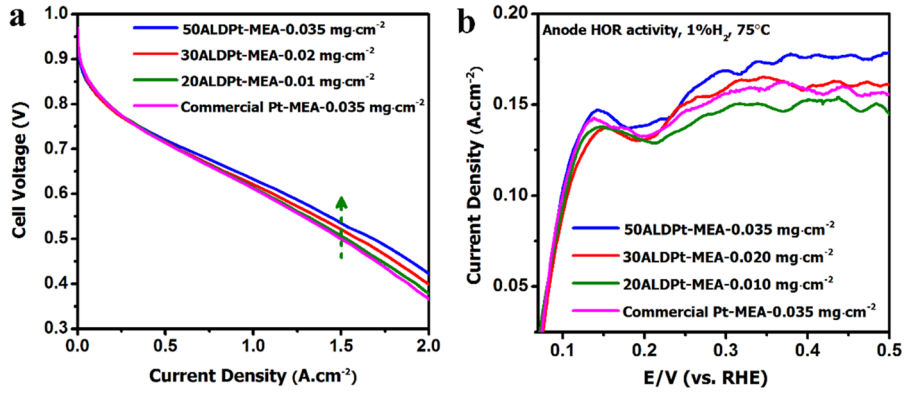

Figure 2. (a) H_2−air polarization curves of ALDPt-MEAs and a commercial Pt-MEA with varied anode Pt loading. (b) *I*−*V* curves of anode catalyst for HOR acquired with the anode as the working electrode (with 1% H_2/N_2 gas feed) and the cathode as the counter electrode (with H_2 feed), scanning from OCV to 0.6 V (vs RHE) at the scan rate of 10 mV s^{-1}.

value of ∼0.954 V (vs RHE). This indicates that no short circuit or gas leakage is occurring during PEMFC operation. In the low current density region (0−0.2 A·cm^{-2}), all the MEAs exhibit a similar high cell voltage. However, when increasing the current density to the ohmic and mass polarization region (>0.7 A·cm^{-2}), an obvious cell voltage difference appears between the ALD Pt-MEAs and the commercial Pt-MEA. The 50ALDPt-MEA with an anode Pt loading of 0.035 mg·cm^{-2} achieves an average cell voltage of 536 mV at the current density of 1.5 mA·cm^{-2}. There is an observed decrease in cell voltage with a reduction in the anode ALDPt loading. It is noteworthy that ALDPt catalysts can achieve much higher performance than the one of the commercial Pt/C with the same Pt loading. When lowering the anode ALDPt loading to 0.02 and 0.01 mg·cm^{-2}, the 30ALDPt-MEA and 20ALDPt-MEA show cell voltages of 522 and 506 mV at a current

DOI: 10.1021/acscatal.8b04504
ACS Catal. 2019, 9, 5365−5374

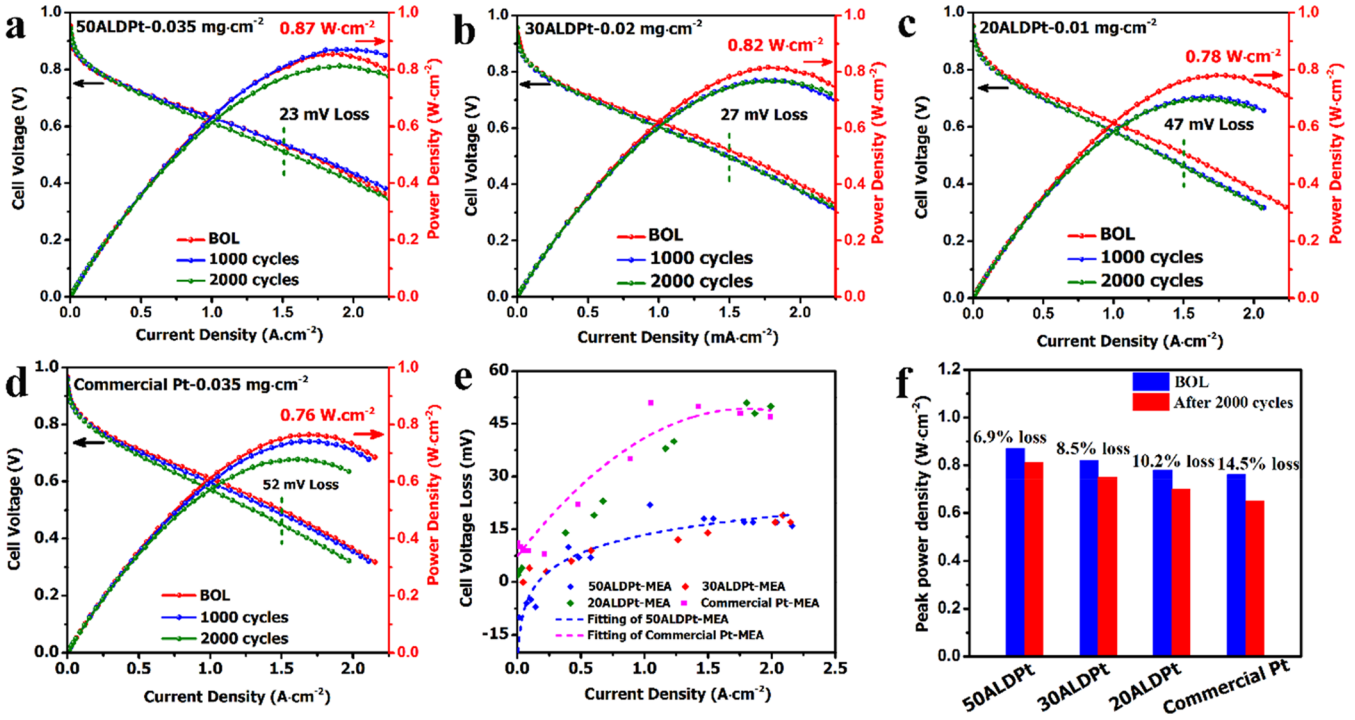

Figure 3. H_2−air PEMFCs polarization and power density curves for MEAs with cathode of 0.4 mg·cm^{-2} commercial Pt/C and anode of (a) 50ALDPt-0.035 mg·cm^{-2}, (b) 30ALDPt-0.02 mg·cm^{-2}, (c) 20ALDPt-0.01 mg·cm^{-2}, and (d) commercial Pt-0.035 mg·cm^{-2}. (e) Relationship between voltage loss and current density for MEAs after 2000 anode potential cycles. (f) Power density of ALDPt-MEAs and commercial Pt-MEA before and after 2000 anode potential cycles (BOL: beginning-of-life).

density of 1.5 mA·cm^{-2}, respectively, higher than the value of 495 mV obtained with commercial Pt-MEA with high Pt loading of 0.035 mg·cm^{-2}. Since this single cell testing variability at 1.5 A·cm^{-2} is ±15 mV (three parallel tests of polarization curves and cell voltage variations are shown in Figure S2), it is believed that the 41 mV cell voltage improvement at 1.5 A·cm^{-2} is attributed to the advantages of 50ALD Pt compared to the commercial Pt/C catalyst at the same Pt loading of 0.035 mg·cm^{-2}. Even with lower Pt loading, the ALD anode can achieve the equivalent or better performance over the conventional Pt/C anode. While using the conventional technology, when the anode Pt loading is lower than 0.035 mg·cm^{-2}, the poor layer uniformity and the thin layer in-plane conductivity could impact MEA performance. Nevertheless, using the ALD technique, ultralow Pt loading (0.01 mg·cm^{-2}) can achieve uniform Pt distribution in the anode carbon surface and the catalyst layer in-plane conductivity will not be impacted.

The mass-transport profile of the ALDPt-MEAs is improved at the high current density region (>1.5 mA·cm^{-2}). We assumed it is due to their structural advantage: the uniformly dispersed Pt NPs display high active surface area of ALD Pt catalyst; the ALDPt NPs are mostly deposited on the carbon layer surface with the efficient Pt-carbon-ionomer three-phase boundary, which shortens the proton pathway and promotes the reactant transport and thus improves the performance, particularly at high current densities. To test anode Pt catalytic activity toward the HOR, the H_2 oxidation polarization curves are determined on the ALDPt-MEAs and commercial Pt-MEA with the anode as the working electrode with 1% H_2/N_2 gas feed and the cathode as the counter electrode with H_2 feed. Figure 2b shows the HOR polarization curves of anode layers with ALDPt-MEAs and commercial Pt-MEA. There are three elementary reaction steps for HOR on the Pt surface, based on the Tafel−Heyrovsky−Volmer mechanism.[5a,b,6b,16] For all the MEAs anodes, the HOR current shows a fast increase at small overpotentials, with the limiting current density of ∼0.15 A·cm^{-2} obtained at an overpotential of ∼0.14 V. Remarkably, the extremely low loading of 20ALDPt-MEA (0.01 mg·cm^{-2}) yielded no noticeable limiting current density loss compared with the high loading commercial Pt catalyst. Therefore, it can be concluded that 20ALDPt-MEA generates extremely low Pt loading but contains comparable specific active sites with the commercial Pt catalyst under higher Pt loading. It is supposed that the high active surface area and small Pt particle size contribute 20ALDPt with significantly enhanced catalytic ability toward the HOR. To understand the real active surface area of Pt in the anode layer, the in situ CO stripping voltammetry on the MEA anode was conducted. As illustrated in Figure S3, the 50ALDPt-MEA with ∼3.2 nm Pt NPs dispersed on the carbon support has an ECSA of 67.4 $m^2 \cdot g^{-1}_{Pt}$, higher than that of 50.3 $m^2 \cdot g^{-1}_{Pt}$ measured for the commercial Pt-MEA under the same Pt loading of 0.035 mg·cm^{-2}. Interestingly, by reducing the ALD cycles to 30 and 20, much higher ECSA of 81.5 and 155 $m^2 \cdot g^{-1}_{Pt}$ could be achieved under the lower Pt loadings of 0.02 and 0.01 mg·cm^{-2}, respectively. The 3 times enhanced ECSA of 20ALDPt catalyst demonstrates the distinct advantage of ALD, which enables the uniform distribution of small Pt NPs on the carbon surface, promoting high Pt active surface area and enhancing the Pt utilization efficiency.

3.3. Stability of PEMFCs Catalyst in Anode Potential Cycles. Like the extensively studied cathode Pt catalyst, the Pt surface area in anode could be gradually reduced in MEA dynamic operations as well, especially in the ultralow Pt loading anodes. Anode potential alternation can occur during

DOI: 10.1021/acscatal.8b04504
ACS Catal. 2019, 9, 5365−5374

Table 1. ECSA Values and Peak Power Density of MEA-BOL before and MEA-EOL after 2000 Cycles AST with ALDPt and Commercial Pt Catalyst in Anode Layers

		ECSA of anode Pt [$m^2 \cdot g^{-1}_{Pt}$]			peak power density [$W \cdot cm^{-2}$]		
anode-MEA	Pt loading in anode/cathode [$mg \cdot cm^{-2}$]	BOL	EOL	loss/%	BOL	EOL	loss/%
50ALDPt-MEA	0.035/0.4	67.4	38.6	42.7	0.87	0.81	6.9
30ALDPt-MEA	0.02/0.4	81.5	41.0	49.7	0.82	0.75	8.5
20ALDPt-MEA	0.01/0.4	155	19.1	88.9	0.78	0.70	10.2
commercial Pt-MEA	0.035/0.4	50.3	9.3	81.5	0.76	0.65	14.5

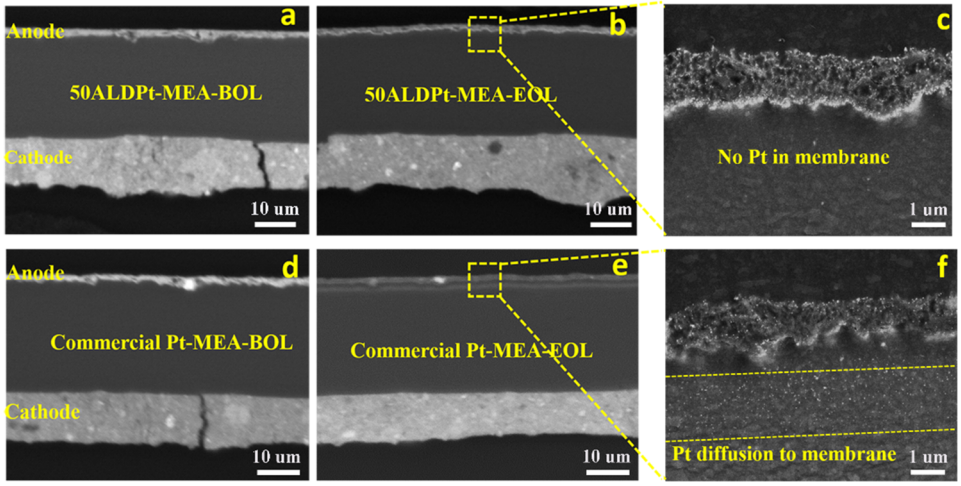

Figure 4. FESEM images of MEA cross sections for (a) 50ALDPt-MEA-BOL and (b, c) 50ALDPt-MEA-EOL after 2000 anode potential cycles AST, (d) commercial Pt-MEA-BOL, and (e, f) commercial Pt-MEA-EOL after 2000 anode potential cycles AST (BOL, beginning-of-life; EOL, end-of-life after 2000 anode potential cycles test).

MEA air/air SUSD cycles, in which the anode potential could vary from ~0 V (in H_2) to >1.0 V (in air). Thus, an investigation into the catalyst stability of the ultralow Pt loading anode in potential cycling becomes important for MEA durability. Anode potential cycling AST was carried out, holding the anode potential at 0.1 V for 30s and then switching to 1.0 V for another 30 s, 60 s for each AST cycle and for a total of 2000 potential cycles. As shown in Figure 3a–d, in the low current density range (0–0.2 $A \cdot cm^{-2}$), little cell voltage loss occurred for both the ALDPt-MEAs and commercial Pt-MEA, which implies that in this potential cycling durability test the cathode ORR kinetics loss is negligible. No significant cathode degradation is observed in this evaluation, as there is no intended cathode stress applied. Due to the fast HOR reaction, the anode performance loss has features similar to those of the Ohmic loss; i.e., the voltage loss shows a linear relationship with the current density. At high current density the anode performance loss becomes more obvious. Figure 3e shows the drop-in cell voltage as a function of current density after 2000 cycles AST, a potential indicator of anode catalyst degradation. It is worth noting that the 50ALDPt-MEA and 30ALDPt-MEA show a relatively low rate of increase in voltage loss with increasing current density after 2000 cycles AST, reaching a maximum and potentially leveling off at ~20 mV. However, with further lowering the Pt loading to 20ALDPt of 0.01 $mg \cdot cm^{-2}$, the voltage loss increases along with the current density and shows a maximum loss of ~50 mV at 2.0 $A \cdot cm^{-2}$, which is comparable to that of the commercial Pt-MEA with higher 0.035 $mg \cdot cm^{-2}$ Pt loading. Through measuring the H_2–air polarization curves of MEAs before and after 2000 cycles AST, it is found that both the ALDPt-MEAs and commercial Pt-MEA display anode catalyst degradation and performance loss. The 50ALDPt-MEA and 30ALDPt-MEA showed much higher BOL peak power densities of 0.87 and 0.82 $W \cdot cm^{-2}$, respectively, decreasing to 0.81 and 0.75 $W \cdot cm^{-2}$. This equates to a 6.9% and 8.5% power density loss after 2000 cycles AST (Figure 3f), respectively, indicating excellent PEMFC performance and durability for the ALDPt catalyst. For 20ALDPt-MEA with 0.01 $mg \cdot cm^{-2}$ extremely low Pt anode loading, the BOL peak power density of 0.78 $W \cdot cm^{-2}$, higher than that of 0.76 $W \cdot cm^{-2}$ for the commercial Pt-MEA with higher Pt loading of 0.035 $mg \cdot cm^{-2}$. The power density of 20ALDPt-MEA decreased to 0.70 $W \cdot cm^{-2}$, a 10.2% loss, better than that of commercial Pt-MEA which degraded from 0.76 to 0.65 $W \cdot cm^{-2}$, representing 14.5% performance loss (Figure 3f). It should be stressed that, to the best of our knowledge, 0.01 $mg \cdot cm^{-2}$ anode Pt loading and 10.2% power loss are the lowest Pt loading and best durability among the reported PEMFC (Table S1 and Figure S4) using Pt catalysts. The outstanding performance and durability of the PEMFC could be attributed to the excellent catalytic activity of the well-dispersed ALDPt NPs and the strong metal–support interaction achieved by ALD.

Analyzing the anode catalyst ECSA of ALDPt-MEAs and commercial Pt-MEA before and after the 2000 cycles AST as indicated in Table 1, it is found that the 50ALDPt-MEA shows BOL ECSA of 67.4 $m^2 \cdot g^{-1}_{Pt}$ much higher than that of 50.3 $m^2 \cdot g^{-1}_{Pt}$ for commercial Pt-MEA (Figure S3). After 2000 cycles AST performed at the anode, the 50ALDPt-MEA shows an anode ECSA of 38.6 $m^2 \cdot g^{-1}_{Pt}$, a 43% loss. This is 4.2 times higher than the 9.3 $m^2 \cdot g^{-1}_{Pt}$ (82% loss) for commercial Pt-MEA, implying much enhanced durability and activity of Pt catalyst achieved through ALD. Furthermore, the ultralow ALDPt of 0.02 and 0.01 $mg \cdot cm^{-2}$ loading exhibit significantly

DOI: 10.1021/acscatal.8b04504
ACS Catal. 2019, 9, 5365–5374

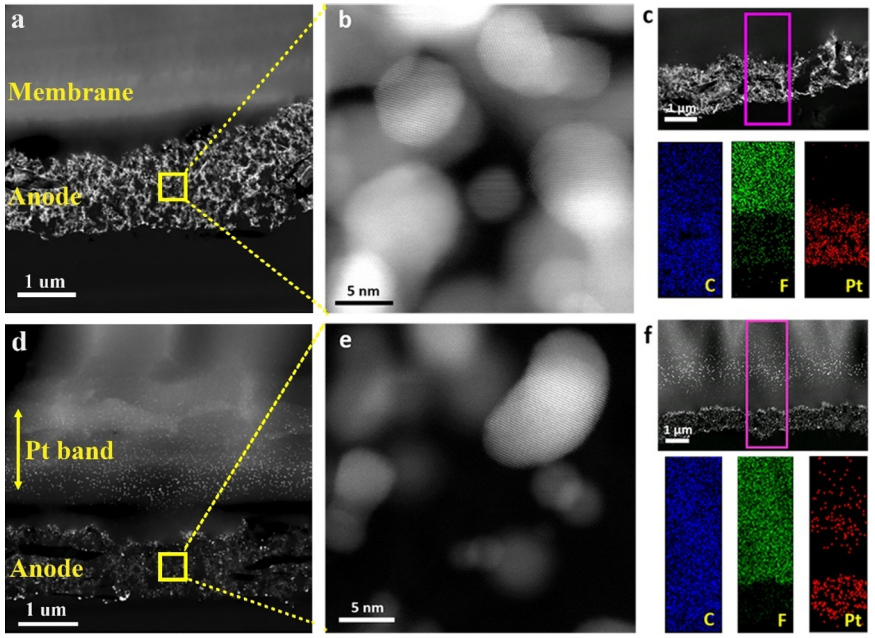

Figure 5. Characterization of cycled MEA cross sections: (a) cross-sectional HAADF-STEM image of the 50ALDPt-MEA-EOL, (b) high-resolution HAADF-STEM image of the Pt catalyst from 50ALDPt-MEA-EOL anode layer, (c) EDX maps of the 50ALDPt-MEA-EOL cross-section, (d) cross-sectional HAADF-STEM image of commercial Pt-MEA-EOL, (e) high-resolution HAADF-STEM image of the Pt catalyst from commercial Pt-MEA-EOL anode layer, and (f) EDX maps of the commercial Pt-MEA-EOL cross-section.

enhanced initial ECSA of 81.5 and 155.0 $m^2 \cdot g^{-1}_{Pt}$, respectively. With continuous potential cycling, the ECSA decreased to 41.0 $m^2 \cdot g^{-1}_{Pt}$ (49% loss) and 19.1 $m^2 \cdot g^{-1}_{Pt}$ (87% loss) for 30ALDPt-MEA and 20ALDPt-MEA, respectively, still higher than the ECSA of 9.3 $m^2 \cdot g^{-1}_{Pt}$ for commercial Pt-MEA. The ECSA loss of anode catalyst is indicative of anode Pt surface degradation during the potential cycling. Additionally, the H_2-pump test was conducted on the MEAs before and after AST to determine the HOR kinetic and to understand the anode loss for each electrode. As shown in Figure S5, the postcycled 50ALDPt anode indicates the same kinetic slope of the HOR with the fresh anode at BOL, only a little decreased limiting current is observed, implying the negligible anode catalyst degradation and high stability of ALDPt during the AST. By contrast, the commercial Pt anode shows an obvious decrease of the HOR kinetic slope and a significantly decreased limiting current after the anode AST, which shows server Pt surface loss and poor stability of commercial Pt catalyst. The anode potential cycling test and ECSA analysis confirm that ALDPt-MEAs even under extremely low Pt loading provide excellent durability in comparison to the commercial Pt-MEA. Based on these results, it is concluded that the ALD technique provides electrode catalysts that not only achieve ultralow Pt loading but also exhibit high catalytic activity, high performance, and excellent durability for PEMFCs applications.

3.4. Cross-Section Analysis of Cycled MEAs. Figure 4 shows cross-sectional SEM images of the ALDPt-MEAs and commercial Pt-MEA before (BOL) and after (EOL) 2000 cycles AST conducted at anode. As shown in the FESEM images, the three distinct layers are the cathode catalyst layer, the anode catalyst layer, and the electrolyte membrane layer between. The thicknesses of the cathode layer and electrolyte membrane layer show little variation before and after the anode potential cycling test, indicating no excessive carbon corrosion of the cathode catalyst layer and no severe thinning of the electrolyte membrane during the anode AST. However, there is a significant difference in the anode/membrane interface for the postcycled ALDPt-MEAs-EOL and the commercial Pt-MEA-EOL. From Figure 4a,b, no significant change is observed in the anode thickness of 50ADLPt-MEA before and after AST. By magnifying the anode/membrane boundary of 50ALDPt-MEA-EOL after potential cycling AST (Figure 4c), no significant Pt particles can be detected in the membrane close to the anode/membrane interface region, although a Pt enriched band can be occasionally observed at the electrode/membrane interface. No detectable Pt particles are observed in this region in any of the cycled ALDPt-MEAs even under ultralow Pt loadings (Figure S6) of 0.02 and 0.01 $mg \cdot cm^{-2}$. This result suggests the ALDPt structure exhibits excellent durability due to the uniformly dispersed particle size and strong ALDPt-carbon interactions. However, for the commercial Pt-MEA, as shown in Figure 4d–f, an obvious Pt band is presented in the membrane close to anode/membrane interface after the potential cycling. This outcome provides unambiguous evidence of commercial Pt surface loss via diffusion of soluble Pt species into the membrane and redeposition of Pt particles in the membrane during the anode potential cycling.[17] Pt migration and subsequent diffusion into the membrane lead to a substantial loss of Pt surface area and lower Pt utilization for catalyzing the HOR in the MEA anode. In contrast, Pt deposition in the membrane is almost undetectable in cycled ALDPt-MEAs, which confirms the performance related observations of significantly enhanced stability of Pt prepared by ALD.

To further investigate the distribution and size change of Pt particles after anode potential cycling AST, TEM images coupled with EDX maps were carried out on the 50ALDPt-MEA and commercial Pt-MEA. Figure 5a shows the HAADF-STEM image of the cross-sectional 50ALDPt-MEA-EOL after anode potential cycling, the membrane is on top of the anode catalyst layer in the image. The HAADF-STEM image is known as a *Z* (atomic number)-contrast image, where the

DOI: 10.1021/acscatal.8b04504
ACS Catal. 2019, 9, 5365–5374

contrast of the image is proportional to the Z number of the elements present in the material. The heavier Pt particles are brighter in the image, while the lighter elements of carbon and fluorine are shown in darker contrast. Clear differences in the membrane close to anode/membrane interface are observed between the 50ALDPt-MEA-EOL sample and commercial Pt-MEA-EOL sample from the cross-sectional STEM images shown in Figure 5a,d. The cross-section of 50ALDPt-MEA-EOL shows minor changes compared to that before AST (as shown in Figure S7), suggesting there is no significant loss of ALDPt in the anode layer after potential cycling. Meanwhile, no detectable Pt particles redeposition is observed in the membrane of the cycled 50ALDPt-MEA, indicating the lab-designed ALDPt-MEA underwent negligible Pt surface loss and exhibited high stability. By contrast, a significant amount of Pt species migration from the anode to the anode/membrane interface and redeposition into the membrane takes place in the commercial Pt-MEA anode layer. Detailed STEM examination of the anode/membrane interface revealed a band of Pt precipitates (Figure 5d) formed in the membrane due to the migration of soluble Pt species into the membrane and then reduced by the H_2 crossed over from the counter electrode (cathode feed with H_2) (Figure S8). This is direct evidence of commercial Pt dissolution and redeposition during the potential cycling AST. In our case by testing the anode in N_2 with the square potential cycling protocol from 0.1 to 1.0 V (vs RHE), the micrometer-scale Pt ions diffusion pronounced the 1.0−1.5 μm Pt redeposition away from the anode/membrane interface. Parts b and e of Figure 5 show the high-resolution STEM images of the Pt particles size in the anode layer of the 50ALDPt-MEA-EOL and commercial Pt-MEA-EOL, revealing the existence of Pt catalyst in the anode after cycling, although the amount of Pt retained can vary. For the commercial Pt-MEA-EOL, a large amount of Pt has diffused into the membrane and only a small portion of the BOL Pt NPs remained in the anode layer, indicating a significant commercial Pt surface loss and degradation. Additionally, the Pt particle size has a wide distribution from 1.5 to 7.0 nm (Figure 5e) in the commercial Pt-MEA-EOL anode layer, due to the Pt migration/coalescence and dissolution/redeposition occurring for the commercial Pt catalyst. The elemental distribution across the anode/membrane interface is further studied by EDX mapping. Figure 5c shows the elemental maps of cycled 50ALDPt-MEA-EOL. As can be seen, C is detected throughout the anode and membrane, Pt is mostly concentrated in the anode layer, a significant amount of F is detected in the membrane, while almost no Pt is observed in the membrane, which is consistent with the STEM results discussed above. The strong chemical interaction between the Pt NPs and carbon support achieved by ALD enables the high stability of the ALDPt catalyst. The elemental maps obtained from the cycled commercial Pt-MEA-EOL sample (Figure 5f) show a clear difference; the Pt is not only concentrated in the anode layer but also detected in the membrane close to the anode/membrane interface, as displayed in the Pt map, which further confirms the sever Pt area loss and the poor stability of commercial Pt catalyst in anode cycling.

Regarding the excellent PEMFC performance and stability indicated by the ALD Pt with extremely low Pt loading, it is discussed that the enhanced performance of ALD Pt is caused by the following factors: (1) The uniformly dispersed Pt particles size achieved by ALD. The uniform dispersion of active nanoparticles should result in a high active surface area and high mass activity of Pt catalyst. The gas−solid self-saturating reaction nature provides ALD with the advantage in preparing Pt NPs in the form of ultasmall particle size and uniform distribution on the carbon surface. The small and uniform particle size guarantee the high surface area of Pt NPs, which contribute the ALDPt with enhanced catalytic activity under the low Pt loading. (2) The strong metal−support interaction between the ALD Pt NPs and carbon support. The chemical deposition of Pt through ALD makes the strong metal−support interactions between the Pt NPs and carbon support, which alleviates the ALDPt particles migration and coalescence on carbon surface, thereby maintaining the high Pt surface area during the potential cycling and achieving the enhanced physical and chemical stability of ALDPt catalyst. However, the origin of excellent stability of ALDPt in resisting Pt dissolution and redeposition under the potential cycling is unclear, which will be examined in future studies.

4. CONCLUSIONS

The deposition of Pt NPs on PEMFC anode carbon layers by ALD has been studied. ALD enables uniform dispersion of the Pt on the carbon surface. Importantly, the Pt particle size and loading can be precisely controlled by the number of ALD cycles. An ALDPt-MEA with an extremely low anode Pt loading of 0.01 mg·cm^{-2} is achieved by 20 ALD cycles, which shows better H_2−air PEMFC performance than a commercial Pt-MEA with a higher Pt loading of 0.035 mg·cm^{-2}. Moreover, the anode potential cycling accelerated stress tests indicate that the ALDPt anode shows much improved durability compared to that of a commercial Pt/C anode. The cycling potential range is between 0.1 and 1.0 V to mimic the anode potential alternation in fuel cell air/air start-up/shutdown processes. The 50ALDPt-MEA exhibits excellent durability with only 8.0% power density loss. Even under the ultralow Pt loading of 0.01 mg·cm^{-2}, the 20ALDPt anode shows an extremely high initial ECSA of 155 $m^2 \cdot g^{-1}_{Pt}$ and power density of 0.78 W·cm^{-2}, with only 10.2% power loss after cycling, which is the lowest anode Pt loading and best durability among the reported PEMFC using Pt catalyst. This research work reveals that the application of ALD for Pt deposition directly on the electrode carbon layers can effectively reduce the Pt loading while enhancing the Pt dispersion, utilization, and durability, even to ultralow anode Pt loading. It is acknowledged that there is still a long road to go to realize the PEMFC widespread application with ultralow Pt loading. Under the fuel starvation and cell reversal mode, an anode can see a higher potential than 1.0 V (vs RHE), which leads to carbon corrosion of anode catalyst and accelerates the degradation of catalyst. Therefore, it is anticipated that developing an excellent catalyst on a corrosion resistant support is required to absolutely avoid permanent damage to the anode electro-catalyst in PEMFC application.

■ ASSOCIATED CONTENT

Supporting Information

The Supporting Information is available free of charge on the ACS Publications website at DOI: 10.1021/acscatal.8b04504.

Additional FESEM, SEM, and TEM images, H_2−air polarization curves, CV and CO stripping I−V curves, table of current state of ultra-low Pt loading in PEMFCs anode, PEMFC peak power density vs anode Pt loading,

DOI: 10.1021/acscatal.8b04504
ACS Catal. 2019, 9, 5365−5374

HOR polarization curves, and schematic of Pt degradation via Pt dissolution (PDF)

AUTHOR INFORMATION

Corresponding Authors

*E-mail: gbotton@mcmaster.ca (G. A. Botton).
*E-mail: ping.he@ballard.com (P. He).
*E-mail: xsun@eng.uwo.ca (X. Sun).

ORCID

Mohammad Norouzi Banis: 0000-0002-6144-6837
Hanshuo Liu: 0000-0001-7745-5407
Siyu Ye: 0000-0002-4384-5025
Gianluigi A. Botton: 0000-0002-8746-1146
Xueliang Sun: 0000-0003-2881-8237

Notes

The authors declare no competing financial interest.

ACKNOWLEDGMENTS

This research was supported by Catalysis Research for Polymer Electrolyte Fuel Cells (CaRPE-FC), Ballard Power Systems Inc., Natural Sciences and Engineering Research Council of Canada (NSERC), Canada Research Chair (CRC) Program, Canada Foundation for Innovation (CFI), Ontario Research Fund (ORF), Automotive Partnership of Canada, and the University of Western Ontario. Part of the electron microscopy characterization was carried out at the Canadian Centre for Electron Microscopy (CCEM), a national facility supported by NSERC, the Canada Foundation for Innovation (via the MSI program) and McMaster University. Z. Song was supported by the Chinese Scholarship Council. We gratefully acknowledge the Ballard scientists Mr. Kyoung Bai, Mr. Alan Young, Dr. Rajesh Bashyam, and Dr. Foroughazam Afsahi help in discussion and analysis of fuel cell performance.

REFERENCES

(1) (a) Debe, M. K. Electrocatalyst approaches and challenges for automotive fuel cells. *Nature* **2012**, *486* (7401), 43−51. (b) Eberle, U.; Muller, B.; von Helmolt, R. Fuel cell electric vehicles and hydrogen infrastructure: status 2012. *Energy Environ. Sci.* **2012**, *5* (10), 8780−8798. (c) Yoshida, T.; Kojima, K. Toyota MIRAI fuel cell vehicle and progress toward a future hydrogen society. *Electrochem. Soc. Interface* **2015**, *24* (2), 45−49. (d) Banham, D.; Ye, S. Current status and future development of catalyst materials and catalyst layers for proton exchange membrane fuel cells: an industrial perspective. *ACS Energy Letters* **2017**, *2* (3), 629−638. (e) Banham, D.; Kishimoto, T.; Zhou, Y.; Sato, T.; Bai, K.; Ozaki, J.-i.; Imashiro, Y.; Ye, S. Critical advancements in achieving high power and stable nonprecious metal catalyst−based MEAs for real-world proton exchange membrane fuel cell applications. *Science advances* **2018**, *4* (3), eaar7180. (f) Cano, Z. P.; Banham, D.; Ye, S.; Hintennach, A.; Lu, J.; Fowler, M.; Chen, Z. Batteries and fuel cells for emerging electric vehicle markets. *Nature Energy* **2018**, *3* (4), 279−289.

(2) (a) Steele, B. C. H.; Heinzel, A. Materials for fuel-cell technologies. *Nature* **2001**, *414*, 345. (b) Stamenkovic, V. R.; Strmcnik, D.; Lopes, P. P.; Markovic, N. M. Energy and fuels from electrochemical interfaces. *Nat. Mater.* **2017**, *16*, 57.

(3) (a) Anderson, R. M.; Yancey, D. F.; Zhang, L.; Chill, S. T.; Henkelman, G.; Crooks, R. M. A theoretical and experimental approach for correlating nanoparticle structure and electrocatalytic activity. *Acc. Chem. Res.* **2015**, *48* (5), 1351−1357. (b) Su, L.; Jia, W.; Li, C. M.; Lei, Y. Mechanisms for Enhanced Performance of Platinum-Based Electrocatalysts in Proton Exchange Membrane Fuel Cells. *ChemSusChem* **2014**, *7* (2), 361−378. (c) Mistry, H.; Varela, A. S.; Kühl, S.; Strasser, P.; Cuenya, B. R. Nanostructured electrocatalysts with tunable activity and selectivity. *Nature Reviews Materials* **2016**, *1*, 16009. (d) Chen, C.; Kang, Y.; Huo, Z.; Zhu, Z.; Huang, W.; Xin, H. L.; Snyder, J. D.; Li, D.; Herron, J. A.; Mavrikakis, M.; Chi, M.; More, K. L.; Li, Y.; Markovic, N. M.; Somorjai, G. A.; Yang, P.; Stamenkovic, V. R. Highly Crystalline Multimetallic Nanoframes with Three-Dimensional Electrocatalytic Surfaces. *Science* **2014**, *343* (6177), 1339−1343.

(4) Fuel Cell Technologies Office. Multi-Year Research, D., and Demonstration Plan. http://energy.gov/sites/prod/files/2016/10/f33/fcto_myrdd_fuel_cells.pdf.

(5) (a) Durst, J.; Simon, C.; Hasché, F.; Gasteiger, H. A. Hydrogen oxidation and evolution reaction kinetics on carbon supported Pt, Ir, Rh, and Pd electrocatalysts in acidic media. *J. Electrochem. Soc.* **2015**, *162* (1), F190−F203. (b) Scofield, M. E.; Zhou, Y.; Yue, S.; Wang, L.; Su, D.; Tong, X.; Vukmirovic, M. B.; Adzic, R. R.; Wong, S. S. Role of chemical composition in the enhanced catalytic activity of Pt-based alloyed ultrathin nanowires for the hydrogen oxidation reaction under alkaline conditions. *ACS Catal.* **2016**, *6* (6), 3895−3908. (c) Neyerlin, K.; Gu, W.; Jorne, J.; Gasteiger, H. A. Study of the exchange current density for the hydrogen oxidation and evolution reactions. *J. Electrochem. Soc.* **2007**, *154* (7), B631−B635. (d) Wang, J. X.; Springer, T. E.; Adzic, R. R. Dual-pathway kinetic equation for the hydrogen oxidation reaction on Pt electrodes. *J. Electrochem. Soc.* **2006**, *153* (9), A1732−A1740. (e) Eom, K.; Kim, G.; Cho, E.; Jang, J. H.; Kim, H.-J.; Yoo, S. J.; Kim, S.-K.; Hong, B. K. Effects of Pt loading in the anode on the durability of a membrane−electrode assembly for polymer electrolyte membrane fuel cells during startup/shutdown cycling. *Int. J. Hydrogen Energy* **2012**, *37* (23), 18455−18462.

(6) (a) Karan, K. Assessment of transport-limited catalyst utilization for engineering of ultra-low Pt loading polymer electrolyte fuel cell anode. *Electrochem. Commun.* **2007**, *9* (4), 747−753. (b) Sheng, W.; Gasteiger, H. A.; Shao-Horn, Y. Hydrogen oxidation and evolution reaction kinetics on platinum: acid vs alkaline electrolytes. *J. Electrochem. Soc.* **2010**, *157* (11), B1529−B1536. (c) Durst, J.; Siebel, A.; Simon, C.; Hasche, F.; Herranz, J.; Gasteiger, H. New insights into the electrochemical hydrogen oxidation and evolution reaction mechanism. *Energy Environ. Sci.* **2014**, *7* (7), 2255−2260. (d) Yun, S. W.; Park, S. A.; Kim, T. J.; Kim, J. H.; Pak, G. W.; Kim, Y. T. Hydrogen Oxidation-Selective Electrocatalysis by Fine Tuning of Pt Ensemble Sites to Enhance the Durability of Automotive Fuel Cells. *ChemSusChem* **2017**, *10* (3), 489−493.

(7) (a) Durst, J.; Orfanidi, A.; Rheinländer, P. J.; Hasché, F.; Eickes, C.; Suchsland, P.; Binder, M.; Gasteiger, H. A. Selective Hydrogen Oxidation Catalyst for Reduced Startup/Shutdown Degradation in Low Temperature Fuel Cells. *ECS Trans.* **2015**, *69* (17), 67−76. (b) Zhang, T.; Wang, P.; Chen, H.; Pei, P. A review of automotive proton exchange membrane fuel cell degradation under start-stop operating condition. *Appl. Energy* **2018**, *223*, 249−262. (c) Qin, C.; Wang, J.; Yang, D.; Li, B.; Zhang, C. Proton exchange membrane fuel cell reversal: a review. *Catalysts* **2016**, *6* (12), 197.

(8) (a) He, P.; Cheng, T.; Bashyam, R.; Young, A. P.; Knights, S. Relative humidity effect on anode durability in PEMFC startup/shutdown processes. *ECS Trans.* **2010**, *33* (1), 1273−1279. (b) Ettingshausen, F.; Kleemann, J.; Marcu, A.; Toth, G.; Fuess, H.; Roth, C. Dissolution and migration of platinum in PEMFCs investigated for start/stop cycling and high potential degradation. *Fuel Cells* **2011**, *11* (2), 238−245.

(9) (a) Zhou, F.; Andreasen, S. J.; Kær, S. K.; Yu, D. Analysis of accelerated degradation of a HT-PEM fuel cell caused by cell reversal in fuel starvation condition. *Int. J. Hydrogen Energy* **2015**, *40* (6), 2833−2839. (b) Jung, J.; Park, B.; Kim, J. Durability test with fuel starvation using a Pt/CNF catalyst in PEMFC. *Nanoscale Res. Lett.* **2012**, *7* (1), 34. (c) Jung, D.-W.; Park, S.; Kim, S.-H.; Kim, J.-B.; Oh, E.-S. Durability of Polymer Electrolyte Membrane Fuel Cell with Pt/CNTs Catalysts in Cell Reversal Conditions by Hydrogen Starvation. *Fuel Cells* **2011**, *11* (6), 866−874. (d) Kang, J.; Jung, D. W.; Park, S.; Lee, J.-H.; Ko, J.; Kim, J. Accelerated test analysis of reversal potential caused by fuel starvation during PEMFCs operation. *Int. J. Hydrogen Energy* **2010**, *35* (8), 3727−3735. (e) Liang, D.; Shen, Q.; Hou, M.;

DOI: 10.1021/acscatal.8b04504
ACS Catal. 2019, 9, 5365−5374

Shao, Z.; Yi, B. Study of the cell reversal process of large area proton exchange membrane fuel cells under fuel starvation. *J. Power Sources* **2009**, *194* (2), 847−853. (f) Taniguchi, A.; Akita, T.; Yasuda, K.; Miyazaki, Y. Analysis of degradation in PEMFC caused by cell reversal during air starvation. *Int. J. Hydrogen Energy* **2008**, *33* (9), 2323−2329.

(10) (a) Dang, D.; Zou, H.; Xiong, Z. a.; Hou, S.; Shu, T.; Nan, H.; Zeng, X.; Zeng, J.; Liao, S. High-performance, ultralow platinum membrane electrode assembly fabricated by in situ deposition of a Pt shell layer on carbon-supported Pd nanoparticles in the catalyst layer using a facile pulse electrodeposition approach. *ACS Catal.* **2015**, *5* (7), 4318−4324. (b) Qayyum, H.; Tseng, C.-J.; Huang, T.-W.; Chen, S.-y. Pulsed Laser Deposition of Platinum Nanoparticles as a Catalyst for High-Performance PEM Fuel Cells. *Catalysts* **2016**, *6* (11), 180. (c) Su, H.-N.; Zeng, Q.; Liao, S.-J.; Wu, Y.-N. High performance membrane electrode assembly with ultra-low platinum loading prepared by a novel multi catalyst layer technique. *Int. J. Hydrogen Energy* **2010**, *35* (19), 10430−10436. (d) Su, H.-N.; Liao, S.-J.; Shu, T.; Gao, H.-L. Performance of an ultra-low platinum loading membrane electrode assembly prepared by a novel catalyst-sprayed membrane technique. *J. Power Sources* **2010**, *195* (3), 756−761.

(11) (a) Dang, D.; Liao, S.; Luo, F.; Hou, S.; Song, H.; Huang, P. A pulse electrochemical deposition method to prepare membrane electrode assemblies with ultra-low anode Pt loadings through in situ construction of active core−shell nanoparticles on an electrode. *J. Power Sources* **2014**, *260*, 27−33. (b) Martin, S.; Martinez-Vazquez, B.; Garcia-Ybarra, P.; Castillo, J. Peak utilization of catalyst with ultra-low Pt loaded PEM fuel cell electrodes prepared by the electrospray method. *J. Power Sources* **2013**, *229*, 179−184. (c) Mougenot, M.; Caillard, A.; Brault, P.; Baranton, S.; Coutanceau, C. High Performance plasma sputtered PdPt fuel cell electrodes with ultra low loading. *Int. J. Hydrogen Energy* **2011**, *36* (14), 8429−8434.

(12) (a) Cheng, N.; Shao, Y.; Liu, J.; Sun, X. Electrocatalysts by atomic layer deposition for fuel cell applications. *Nano Energy* **2016**, *29*, 220−242. (b) Cheng, N.; Banis, M. N.; Liu, J.; Riese, A.; Li, X.; Li, R.; Ye, S.; Knights, S.; Sun, X. Extremely stable platinum nanoparticles encapsulated in a zirconia nanocage by area-selective atomic layer deposition for the oxygen reduction reaction. *Adv. Mater.* **2015**, *27* (2), 277−281. (c) Cheng, N.; Stambula, S.; Wang, D.; Banis, M. N.; Liu, J.; Riese, A.; Xiao, B.; Li, R.; Sham, T.-K.; Liu, L.-M. Platinum single-atom and cluster catalysis of the hydrogen evolution reaction. *Nat. Commun.* **2016**, *7*, 13638. (d) Kim, H. G.; Lee, H.-B.-R. Atomic Layer Deposition on 2D Materials. *Chem. Mater.* **2017**, *29* (9), 3809−3826.

(13) (a) George, S. M. Atomic Layer Deposition: An Overview. *Chem. Rev.* **2010**, *110* (1), 111−131. (b) Sobel, N.; Hess, C. Nanoscale Structuring of Surfaces by Using Atomic Layer Deposition. *Angew. Chem., Int. Ed.* **2015**, *54* (50), 15014−15021. (c) Meng, X.; Wang, X.; Geng, D.; Ozgit-Akgun, C.; Schneider, N.; Elam, J. W. Atomic layer deposition for nanomaterial synthesis and functionalization in energy technology. *Mater. Horiz.* **2017**, *4* (2), 133−154. (d) Lu, J.; Elam, J. W.; Stair, P. C. Atomic layer deposition—Sequential self-limiting surface reactions for advanced catalyst "bottom-up" synthesis. *Surf. Sci. Rep.* **2016**, *71* (2), 410−472. (e) Lu, J.; Elam, J. W.; Stair, P. C. Synthesis and Stabilization of Supported Metal Catalysts by Atomic Layer Deposition. *Acc. Chem. Res.* **2013**, *46* (8), 1806−1815.

(14) (a) Sun, S.; Zhang, G.; Gauquelin, N.; Chen, N.; Zhou, J.; Yang, S.; Chen, W.; Meng, X.; Geng, D.; Banis, M. N. Single-atom catalysis using Pt/graphene achieved through atomic layer deposition. *Sci. Rep.* **2013**, *3*, 1775. (b) Cheng, N.; Liu, J.; Banis, M. N.; Geng, D.; Li, R.; Ye, S.; Knights, S.; Sun, X. High stability and activity of Pt electrocatalyst on atomic layer deposited metal oxide/nitrogen-doped graphene hybrid support. *Int. J. Hydrogen Energy* **2014**, *39* (28), 15967−15974.

(15) Cheng, N.; Banis, M. N.; Liu, J.; Riese, A.; Mu, S.; Li, R.; Sham, T.-K.; Sun, X. Atomic scale enhancement of metal−support interactions between Pt and ZrC for highly stable electrocatalysts. *Energy Environ. Sci.* **2015**, *8* (5), 1450−1455.

(16) Montero, M. A.; Fernández, J. L.; Gennero de Chialvo, M. R.; Chialvo, A. C. Kinetic Study of the Hydrogen Oxidation Reaction on Nanostructured Iridium Electrodes in Acid Solutions. *J. Phys. Chem. C* **2013**, *117* (48), 25269−25275.

(17) (a) Takao, S.; Sekizawa, O.; Nagamatsu, S. i.; Kaneko, T.; Yamamoto, T.; Samjeské, G.; Higashi, K.; Nagasawa, K.; Tsuji, T.; Suzuki, M. Mapping platinum species in polymer electrolyte fuel cells by spatially resolved XAFS techniques. *Angew. Chem., Int. Ed.* **2014**, *53* (51), 14110−14114. (b) Holby, E. F.; Sheng, W.; Shao-Horn, Y.; Morgan, D. Pt nanoparticle stability in PEM fuel cells: influence of particle size distribution and crossover hydrogen. *Energy Environ. Sci.* **2009**, *2* (8), 865−871. (c) Ferreira, P.; Shao-Horn, Y.; Morgan, D.; Makharia, R.; Kocha, S.; Gasteiger, H. *J. Electrochem. Soc.* **2005**, *152* (11), A2256−A2271.

DOI: 10.1021/acscatal.8b04504
ACS Catal. 2019, 9, 5365−5374